C.-K. Fang
Associate Professor.
Department of Mechanical Engineering,
China Institute of Technology
and Commerce,
Nankang, Taipei, Taiwan, R.O.C.

E. Kannatey-Asibu Jr.
Professor

J. R. Barber
Professor.

Department of Mechanical Engineering
and Applied Mechanics,
University of Michigan,
Ann Arbor, MI 48109

Far-Field Initial Response of Acoustic Emission From Cracking in a Weldment

An analytical expression is developed for the relationship between far-field acoustic emission (AE) signal and the propagation of a finite plane crack due to a nonuniform residual stress in a weldment. The AE sensor is situated at the boundary parallel to the crack surface. The quasi-static crack opening displacement (COD) rate is used as the source function. The AE initial response on a traction-free surface is obtained as a function of instantaneous crack length and speed. A closed-form expression is obtained for the normal surface displacement at the epicenter when the crack propagates at uniform speed for a finite duration between initiation and arrest. Results from an earlier analysis of the (variable) speed of crack propagation in a weldment are used to develop a more exact numerical prediction of the surface motion. The effects of initial crack length and bluntness on AE surface motion are investigated in both time and frequency domains.

1 Introduction

The problems of weldment cracks and structural integrity are of major concern to many industries, including the automotive, shipbuilding, nuclear power, aircraft, and other industries where pressure vessels are extensively used. Structural failure in such areas can sometimes be catastrophic, either by virtue of the failure or the impact of the contents of the structure on its environment.

Such failures could result from defects that exist in the material from which the part is made or those that are introduced during fabrication. The greatest possible source of failure is the presence of flaws such as cracks. Cracks in weldments can be formed during the welding process itself or later as a result of residual stress and martensite formed during cooling. Unfortunately, conventional nondestructive evaluation (NDE) techniques are either inapplicable or too expensive to provide real time monitoring of crack formation and propagation. Acoustic emission sensing, however, is well suited to such an application.

AE is a transient elastic wave generated by the rapid release of energy within a material (Liptai and Tatro, 1976). The AE generated during micro-cracking has been studied by many researchers (Rice, 1980; Wadley et al., 1981; Ohtsu and Ono, 1984; Wakayama and Kishi, 1985; Ohtsu et al., 1987; Enoki and Kishi, 1988; Enoki et al., 1986, 1990), in which the crack was viewed as a point source, which is valid if the crack region is small compared with (1) the distance between the field point and the source, and (2) the shortest wavelength of the stress wave. Previously, modeling of the dynamic response due to the propagation of the main crack has not been well studied. Although the main crack can be modeled as a point source if the body is relatively large, the result might be invalid for high frequencies. This is because the wave length for high frequency AE might not be able to fulfill the second condition for the point source approximation.

AE generated during the propagation of macro-cracking has been modeled as microcracking occurring in front of the main crack. This approach was utilized in the study of pop-in fracture in stable crack growth due to the coalescence of voids formed during plastic blunting of the macrocrack tip prior to crack initiation (Kishi and Ohira, 1983); microcracking during stable crack growth in fracture toughness testing of alumna ceramics (Wakayama and Kishi, 1985); and microcrack formation in front of a propagating fatigue crack (Chen and Sachse, 1988). However, it might not be suitable for unstable brittle fracture. Furthermore, this model does not consider the opening of the main crack due to relaxation as the total crack length is increased. From the experimental results for compact tension specimens, Wadley and Scruby (1983) found that the relaxation of the main crack had a more significant impact on the amplitude and life time of source function than that due to microcracking itself. Consequently, in the modeling of AE in a finite-crack problem, the propagation and opening of the entire crack need to be considered.

Under the assumption of linearity, the surface motion at sensor site is a convolution of a source function and structure function. The former contains the dynamic information about the source event, while the latter carries that of wave propagation in the medium. In the microcracking (point source) problem, the source function can be a moment tensor and the structure function is a spatial derivative of the Green's function. For a finite crack, the moment "density" tensor needs to be employed instead of moment tensor (an integration of moment density tensor over crack area). And integration of the convolution of moment density tensor and the spatial derivative of the Green's function needs to be carried out over the entire crack area. The moment density function can be expressed as a function of COD. This COD depends on stress distribution and instantaneous crack length.

Because a suitable crack-tip equation of motion has not been available until recently, it was impossible to describe the instantaneous crack length precisely as a function of time. Previously, a constant crack speed approximation has been used to obtain the COD and elastodynamic response (Hirose and Achenbach, 1991). Conventionally, Seismologists have assumed constant fault speed in the modeling of source mechanisms, and related it to the signals from seismograms. This assumption, however, is probably inaccurate, particularly in the case of a weldment, where the residual stress is nonuniformly distributed. This question was investigated in a recent paper (Fang et al., 1993b), where a crack-tip equation of motion was derived and used to obtain predictions of the instantaneous crack length.

In this research, we study the vertical motion of an AE sensor due to the initiation and propagation of a finite crack under a nonuniform residual stress in a weldment. It is assumed that

Contributed by the Manufacturing Engineering Division for publication in the JOURNAL OF MANUFACTURING SCIENCE AND ENGINEERING. Manuscript received Oct. 1993; revised April 1995. Technical Editor: S. Kapoor.

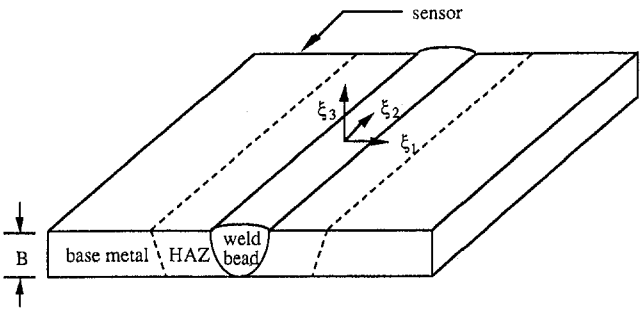

Fig. 1 Weldment configuration

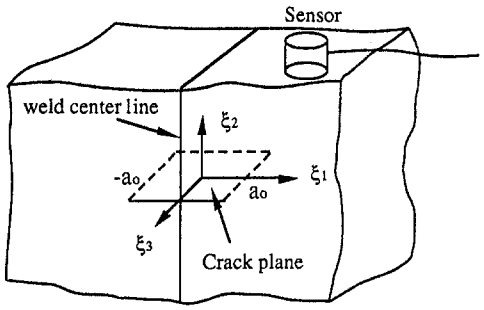

Fig. 2 The rectangular crack in the weldment

the weldment is homogeneous and isotropic. Since we are addressing the cold cracking problem, it is also assumed that the weldment has cooled to the temperature range in which linear elastodynamics is applicable. We employ the relation between the surface motion and COD developed by Fang et al. (1993a), which utilized the Green's function in an infinite body and consider the first reflection on the free boundary. Consequently, the result is independent of structure geometry, but is restricted to the initial period of motion before reflections from the remote boundaries have had time to reach the sensor location. The quasi-static crack opening displacement (COD) rate was used as the source function.

Through integration of the convolution of the source and Green's function mentioned above, we derive the AE surface motion as a function of instantaneous crack length and speed. For comparison, a constant crack speed model is utilized to derive the first vertical motion in closed form. We then employ the variable crack speed model (Fang et al., 1993b) to simulate the surface motion numerically. Based on the latter model, we also investigate the dependence of surface motion on initial crack length and bluntness parameter in both time and frequency domains.

2 Statement of the Problem

Consider a weldment of thickness B, as shown in Fig. 1, subjected to a non-uniformly distributed longitudinal residual stress in the ξ_2-direction due to the shrinkage of the material during the cooling process. An initial through crack, of a length $2a_0$, starts to propagate in the ξ_1-ξ_3 plane, as shown in Fig. 2, as a result of the build up of the tensile residual stress σ_{22}. An AE sensor is placed on the edge surface of the weldment parallel to the crack plane to detect the propagation of the crack. Figure 3 shows the coordinate system used to define the problem. The crack is located in the plane $\xi_2 = 0$ which is denoted by Γ, and a source element of this surface, $d\Gamma$, has position vector $\boldsymbol{\xi}$. A general field point is defined by position vector $\mathbf{x}$ and the vector

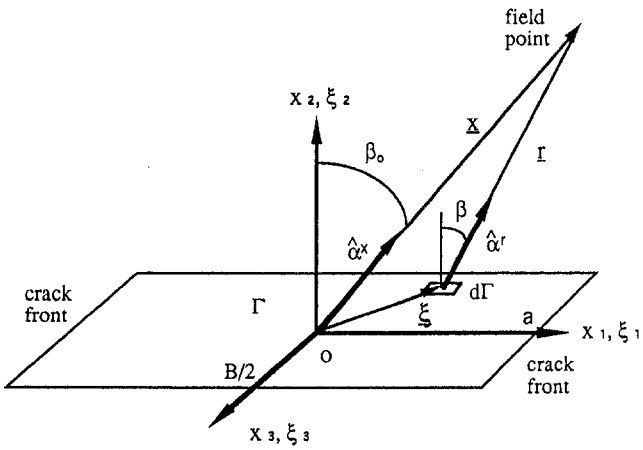

Fig. 3 Configuration of the rectangular crack surface and field point

Nomenclature

a = instantaneous crack half length
a_o = initial crack half length
a_f = final crack half length
B = width of the crack in the x_3-direciton, plate thickness
c = half width of the tension zone of residual stress
C_d, C_s = longitudinal (P-wave) and shear wave (S-wave) speeds
E = Young's modulus
f = frequency
$H(t)$ = unit Heaviside step function
h = depth of the crack below the free surface
K_{IO} = fracture toughness for the initiation of a perfectly sharp crack
K'_{IO} = fracture toughness for the initiation of a blunt crack or apparent fracture toughness
n_b = bluntness parameter
$P'P\hat{}$ = Fresnel coefficient for P-wave due to P-wave incidence
$P'S\hat{}$ = Fresnel coefficient for S-wave due to P-wave incidence
$\mathbf{r} = \mathbf{x} - \boldsymbol{\xi}$
$r = |\mathbf{x} - \boldsymbol{\xi}|$, distance between field and source points
T = duration of crack propagation
t = time
$t' = = t - (h/C_d)$
u_v = normal displacement on the free surface
$\dot{u}_v$ = normal velocity on the free surface
v = crack speed
v_0 = constant crack speed
$\mathbf{x}$ = field point
$x = |\mathbf{x}|$
x_i = rectangular coordinates
$\boldsymbol{\alpha}^r$ = unit vector of $\mathbf{r}$
$\boldsymbol{\alpha}^x$ = unit vector of $\mathbf{x}$
$\hat{\boldsymbol{\alpha}}^{\xi}$ = unit vector of $\boldsymbol{\xi}$
β = the angle between $\boldsymbol{\alpha}^r$ and $\hat{\boldsymbol{\xi}}_2$
β_0 = the angle between $\boldsymbol{\alpha}^x$ and $\hat{\boldsymbol{\xi}}_2$
Γ = crack plane
Δu = crack opening displacement
$\Delta \dot{u}$ = crack opening rate
$\delta(t)$ = Dirac delta function of time
$\theta = \cos^{-1}(\xi_1/a)$
θ_i = angle of incidence
θ_{ps} = reflective angles of the $P'S\hat{}$ wave
λ = Lame constant
λ_w = wave length
μ = Lame constant (shear modulus)
$\boldsymbol{\xi}$ = source point
$\xi = |\boldsymbol{\xi}|$
ξ_i = rectangular coordinates
ρ = density
σ_0 = maximum tensile residual stress
σ_R = magnitude of residual stress
σ_{ij} = stress tensor
ω = circular frequency

$\mathbf{r} = (\mathbf{x} - \boldsymbol{\xi})$ therefore defines the position of the field point relative to the source element. The magnitudes of the vectors $\boldsymbol{\xi}$, $\mathbf{x}$, $\mathbf{r}$ are denoted by ξ, x, r, respectively, and the corresponding unit vectors by $\boldsymbol{\alpha}^{\xi}$, $\boldsymbol{\alpha}^{x}$, $\boldsymbol{\alpha}^{r}$. The angle between the vectors $\boldsymbol{\alpha}^{r}$ and $\boldsymbol{\xi}_2$ is denoted by β. The instantaneous crack length is denoted by 2a. During crack propagation, stress waves are generated from the crack source and reach the field point. The stress waves are detectable if the field point is on a free boundary. We will derive the initial response on the boundary.

3 Far-Field Initial Surface Motion in a Finite Body

We first investigate the far-field initial response of AE due to the variation of COD during the propagation of a rectangular crack in a finite plate. We note that the *S*-waves arrive later than the *P*-waves, and might therefore be contaminated by the secondary reflections of dilatational waves before they reach the sensor site in a finite body. Consequently, we only consider the *P*-wave response. Although there might be large grains in the weldment, it does not make a big difference if the grain size is much smaller than the wave lengths of interest. The phases in the heat affected zone (HAZ) and the base metal in the weldment might be different, and thus the material properties and hence wave speeds might vary with location and direction. However, the wave speeds are not very sensitive to microstructure or even to carbon content over a range of steels and hence the errors associated with the assumption of isotropy and homogeneity are unlikely to be significant.

Far-field response due to the propagation of displacement discontinuity in an "infinite" body can be found in Aki and Richards (1980). It needs to be modified to obtain "surface" displacement by considering reflection and mode conversion. Alternatively, we used Fang's (1993a) result for complete-field surface motion as a function of the variation of COD, $\Delta u(\xi, t)$, with time t. It is a superposition of the normal motion due to the incidence of the P wave and that due to the incident S waves. Although the result was derived for a half-space, it is also valid for the initial response in a finite body before secondary reflections reach the field point of interest. We simplified the result to far-field surface displacement due to the arrival of *P*-wave only. For far-field consideration, the distance from the crack to the sensor, r, is much larger than the longest wavelength of the disturbance and the linear dimensions of the source (Rice, 1980). Let λ_w be wave lengths of stress waves. Since $\lambda_w/r \ll 1$ for far-field response, Fang's (1993a) result for normal surface displacement becomes

$$u_v = \frac{[\lambda + 2\mu \cos^2\beta]}{4\pi\rho C_d^3} \times \int_\Gamma \frac{1}{r} \Delta\dot{u}\left(\boldsymbol{\xi}, t - \frac{r}{C_d}\right) E^{(p)}(\theta_i) d\Gamma(\boldsymbol{\xi}), \quad (1)$$

where λ and μ are Lame constants, ρ is the density of the material, C_d the longitudinal wave speed, $\Delta\dot{u}$ the time derivative of Δu, or crack opening rate,

$$E^{(p)}(\theta_i) = [1 - P'P`] \cos\theta_i + P'S` \sin\theta_{ps}, \quad (2)$$

with the Fresnel coefficients

$$P'P` = \frac{4\left(\frac{\sin\theta_i}{C_d}\right)^2 \frac{\cos\theta_i}{C_d}\frac{\cos\theta_{ps}}{C_s} - \left[\frac{1}{C_s^2} - 2\left(\frac{\sin\theta_i}{C_d}\right)^2\right]^2}{4\left(\frac{\sin\theta_i}{C_d}\right)^2 \frac{\cos\theta_i}{C_d}\frac{\cos\theta_{ps}}{C_s} + \left[\frac{1}{C_s^2} - 2\left(\frac{\sin\theta_i}{C_d}\right)^2\right]^2} \quad (3)$$

and

$$P'S` = \frac{4\frac{\sin\theta_i}{C_d}\frac{C_d}{C_s}\frac{\cos\theta_i}{C_d}\left[\frac{1}{C_s^2} - 2\left(\frac{\sin\theta_i}{C_d}\right)^2\right]}{4\left(\frac{\sin\theta_i}{C_d}\right)^2 \frac{\cos\theta_i}{C_d}\frac{\cos\theta_{ps}}{C_s} + \left[\frac{1}{C_s^2} - 2\left(\frac{\sin\theta_i}{C_d}\right)^2\right]^2}, \quad (4)$$

$\theta_{ps} = \sin^{-1}((C_s/C_d)\sin\theta_i)$, C_s = shear wave speed, and θ_i the angle of incidence, which is restricted to the range:

$$\theta_i < \sin^{-1}\sqrt{\frac{\mu}{\lambda + 2\mu}}, \quad (5)$$

to avoid surface wave effects (Fang et al., 1993a).

Since the crack plane is parallel to the boundary surface where the AE sensor is located, $\theta_i = \beta$. We note that β is a function of ξ and can be expressed as

$$\beta = \cos^{-1}\frac{\sqrt{(x_1 - \xi_1)^2 + (x_3 - \xi_3)^2}}{r} = \cos^{-1}\frac{\sqrt{x_1^2 + x_3^2}}{r}\left[1 + O\left(\frac{\xi_1}{r}, \frac{\xi_3}{r}\right)\right]. \quad (6)$$

For far-field assumption, the crack is very small in comparison with the distance to the sensor, i.e., max. $\{a, B/2\}/r \ll 1$, or max. $\{\xi_1/r, \xi_3/r\} \ll 1$, the bracketed term in the above equation reduces to unity. It then follows that

$$\beta \approx \beta_o = \cos^{-1}\frac{\sqrt{x_1^2 + x_3^2}}{r} \quad (7)$$

(see Fig. 3), and $E^{(p)}(\beta) \approx E^{(p)}(\beta_0)$. In addition, since

$$r \approx x - [\hat{\boldsymbol{\alpha}}^x \cdot \boldsymbol{\xi}], \quad (8)$$

if

$$\max.(\xi^2) \ll \frac{x\lambda_w}{2} \quad (9)$$

(Aki and Richards, 1980), Eq. (1) becomes

$$u_v = \frac{[\lambda + 2\mu\cos^2\beta_o]E^{(p)}(\beta_o)}{4\pi\rho x C_d^3} \times \int_\Gamma \Delta\dot{u}\left(\boldsymbol{\xi}, t - \frac{x - [\hat{\boldsymbol{\alpha}}^x \cdot \boldsymbol{\xi}]}{C_d}\right) d\Gamma(\boldsymbol{\xi}), \quad (10)$$

where the "r" in the denominator in Eq. (1) has been further replaced by "x" [see Eq. (8)], while the "r" in the retarded time r/C_d in the integrand cannot, since small differences in arrival times from different locations on the crack plane can have a significant effect on the resultant waveform.

The two conditions $\lambda_w/r \ll 1$ and max. $\{a, B/2\}/r \ll 1$ define the "far-field assumption." For a rectangular crack as shown in Fig. 3, the maximum ξ occurs at $\xi_1 = \pm a$, $\xi_3 = \pm B/2$, giving $\xi = \sqrt{a^2 + B^2/4}$. Thus (9) can be written as $x \gg 2[a^2 + B^2/4]/\lambda_w$, or

$$\frac{2[a^2 + B^2/4]}{x^2} \ll \frac{\lambda_w}{x}. \quad (11)$$

Combining the far-field conditions and (11), we have

$$\frac{2[a^2 + B^2/4]}{x^2} \ll \frac{\lambda_w}{x} \ll 1, \quad (12)$$

or

$$x \gg \max.\left[\lambda_w, \frac{2[a^2 + B^2/4]}{\lambda_w}\right]. \quad (13)$$

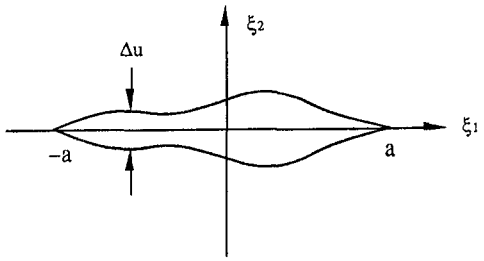

Fig. 4 Crack opening in an arbitrary stress field

We note that the wavelength in steels is about 15–120 mm for the AE signals with frequencies 50–400 kHz. If the crack length is 60 mm (a = 30 mm) and the thickness of the plate is 10 mm, we require $x \gg 123$ mm.

Since $\hat{\boldsymbol{\alpha}}^x = (x_1, x_2, x_3)/x$ and $\boldsymbol{\xi} = (\xi_1, 0, \xi_3)$ as shown in Fig. 3, Eq. (8) becomes

$$r \approx x - [x_1\xi_1 + x_3\xi_3]/x. \tag{14}$$

Employing the above equation and introducing the limits of integration, the displacement field given by Eq. (10) becomes

$$u_v = \frac{[\lambda + 2\mu \cos^2 \beta_o]E^{(p)}(\beta_o)}{4\pi\rho x C_d^3} \times \int_{-B/2}^{B/2}\int_{-a}^{a} \Delta\dot{u}\left(\boldsymbol{\xi}, t - \frac{x^2 - x_1\xi_1 - x_3\xi_3}{xC_d}\right)d\xi_1 d\xi_3. \tag{15}$$

This equation defines the initial vertical surface motion at (x_1, x_2, x_3) far away from the source due to crack propagation, the restriction for the sensor location and angle of incidence being given by the inequalities (13) and (5), respectively. The unknown crack opening rate $\Delta\dot{u}$ will be derived in the next section.

4 Source Function: Quasi-static Crack Opening

In this section, we investigate the crack opening during crack propagation due to the residual stress in the weldment. Masubuchi (1960) developed an analytical method of determining the quasi-static COD due to a given distribution of residual stress.

Figure 4 depicts a two-dimensional straight through crack of length $2a$ occurring along the ξ_1-axis. Let $\theta = \cos^{-1}(\xi_1/a)$, $0 \le \theta \le \pi$. The relationship between the crack opening displacement Δu and the residual stress distribution $\sigma_R(\xi_1)$ on the crack line before the presence of the crack is given (Masubuchi, 1960) by

$$\Delta u(\theta, a) = \sum_{p=1}^{\infty} A_p(a) \sin(p\theta), \tag{16}$$

where

$$A_p(a) = \frac{8a}{\pi E p}\int_o^{\pi} \sigma_R \sin(p\theta) \sin\theta d\theta, \tag{17}$$

and E is the Young's modulus. In the situation where σ_R is uniform with magnitude σ_0, Eq. (16) reduces to the well-known expression for COD under uniform loading conditions (Broek, 1986; Barber, 1992)

$$\Delta u(\xi_1) = \frac{4\sigma_o}{E}\sqrt{a^2 - \xi_1^2}, \quad \text{for} \quad |\xi_1| \le a, \xi_2 = 0. \tag{18}$$

Now consider the case in a weldment. Experimental data for the longitudinal residual stress σ_R in a butt weld joint were given by Masubuchi (1960), Masubuchi and Martin (1966), and Tatsukawa (1972). The tensile residual stress responsible for cracking can be approximated by the parabolic distribution

$$\sigma_R(\xi_1) = \begin{cases} \sigma_o\left\{1 - \left[\dfrac{\xi_1}{c}\right]^2\right\} & |\xi_1| \le c \\ 0 & |\xi_1| \ge c \end{cases} \tag{19}$$

(Masubuchi, 1960) where σ_0 is the maximum tensile residual stress at the weld center and c is the half width of the tension zone of the longitudinal residual stress. Introducing Eq. (19) into Eqs. (17) and (16), we obtain

$$\Delta u(\theta, a) = \frac{4\sigma_o}{E}\left\{\left[a - \frac{a^3}{4c^2}\right]\sin\theta - \frac{a^3}{12c^2}\sin 3\theta\right\}, \tag{20}$$

where

$$\sigma_o = \frac{2c^2 K_{IO}}{2c^2 - a_o^2}\sqrt{\frac{n_b}{\pi a_o}} \tag{21}$$

for crack initiation, n_b is the bluntness parameter defined as $(K'_{IO}/K_{IO})^2$ (Fang et al., 1993b), K'_{IO} is the apparent fracture toughness (the crack tip can be blunt) and K_{IO} is the corresponding value for a perfectly sharp crack.

Differentiating Eq. (20) with respect to time and writing $v = da/dt$ for the rate of crack extension, we have

$$\Delta\dot{u}(\boldsymbol{\xi}, t) = \frac{4\sigma_o v(t) a(t)}{E\sqrt{[a(t)]^2 - \xi_1^2}}\left\{1 - \frac{[a(t)]^2}{2c^2}\right\} \tag{22}$$

for the crack opening rate.

5 Surface Motion Due to Crack Propagation in a Weldment

The crack opening rate, $\Delta\dot{u}$, of Eq. (22) can be substituted into Eq. (15) to derive the initial surface motion due to crack propagation, giving

$$u_v(t) = \frac{2K_{IO}[\lambda + 2\mu\cos^2\beta_o]E^{(p)}(\beta_o)}{\rho x E[2 - (a_o/c)^2]C_d^3}\sqrt{\frac{n_b}{\pi^3 a_o}}\int_{-B/2}^{B/2}\int_{-a}^{a} \times \frac{v\left(t - \dfrac{x^2 - x_1\xi_1 - x_3\xi_3}{xC_d}\right) a\left(t - \dfrac{x^2 - x_1\xi_1 - x_3\xi_3}{xC_d}\right)}{\sqrt{\left[a\left(t - \dfrac{x^2 - x_1\xi_1 - x_3\xi_3}{xC_d}\right)\right]^2 - \xi_1^2}} \times \left\{1 - \frac{\left[a\left(t - \dfrac{x^2 - x_1\xi_1 - x_3\xi_3}{xC_d}\right)\right]^2}{2c^2}\right\} d\xi_1 d\xi_3. \tag{23}$$

This equation is valid for the initial motion due to a rectangular through crack propagating symmetrically in the $\pm\xi_1$-direction with an arbitrary crack speed. The sensor can be at arbitrary point on the boundary parallel to the crack plane, as shown in Fig. 5, with restrictions given by the inequalities (13) and

$$\beta_o < \sin^{-1}\sqrt{\frac{\mu}{\lambda + 2\mu}}. \tag{24}$$

However, numerical integration in Eq. (23) is necessary except at the epicenter.

To get an analytical result, we consider the special case where the vertical surface displacement u_v is determined at the epicenter $(0, h, 0)$. In this case, $x = h$, $\beta_o = 0$, $\theta_{ps} = 0$, $P'P^{\wedge} = -1$, $P'S^{\wedge} = 0$, and thus $E^{(p)}(\beta_o) = 2$. Substituting these results

into (23) we obtain the normalized (dimensionless) vertical surface displacement as

$$\frac{u_v(t)}{D} = \frac{\sqrt{n_b}}{[2-(a_o/c)^2]\sqrt{a_o/c}} \frac{v(t')}{C_d} \times \left\{ \left[\frac{a(t')}{c} \right] - \frac{1}{2} \left[\frac{a(t')}{c} \right]^3 \right\}, \quad (25)$$

where $t' = t - (h/C_d)$, and the normalization factor

$$D = \frac{4BK_{IO}\sqrt{c}}{hE\sqrt{\pi}}. \quad (26)$$

6 Results and Discussion

Equation (25) can be used to predict the vertical surface displacement if the crack length is a known function of time. In general this depends on an analysis of the dynamic fracture process at the crack tip (Fang et al., 1993b) and requires numerical solution. This case will be considered below in Section 6.2, but we first consider the simpler case of constant speed crack propagation, for which a closed form solution of Eq. (25) is possible.

6.1 Constant Crack Speed. Suppose that an initially sharp crack ($n_b = 1$) of half length a_o starts to propagate at time $t = 0$ and propagation continues at constant speed v_o until arrest occurs at $t = T$. It follows that the instantaneous half length and speed are defined by

$$a(t) = a_o + v_o[tH(t) - [t-T]H(t-T)], \quad (27a)$$

$$v(t) = v_o[H(t) - H(t-T)], \quad (27b)$$

where $H(t)$ is the unit Heaviside step function. It also follows that the crack half length at arrest is $a_f = a_o + v_oT$. Substituting Eqs. (27a), (27b), and $n_b = 1$ into (25), we obtain

$$\frac{u_v(t)}{D} = \frac{v_o}{C_d[2-(a_o/c)^2]\sqrt{a_o/c}} \left\{ \left[\frac{a_o + v_o t'}{c} \right] - \frac{1}{2} \left[\frac{a_o + v_o t'}{c} \right]^3 \right\} [H(t') - H(t'-T)]. \quad (28)$$

The corresponding vertical surface velocity can be obtained by differentiating Eq. (29) with respect to time and is

$$\frac{\dot{u}_v(t)}{D} = \frac{v_o}{C_d[2-(a_o/c)^2]\sqrt{a_o/c}} \times \left\{ \left\{ \frac{v_o}{c} - \frac{3v_o}{2c} \left[\frac{a_o + v_o t'}{c} \right]^2 \right\} [H(t') - H(t'-T)] \right.$$

$$\left. + \left\{ \left[\frac{a_o + v_o t'}{c} \right] - \frac{1}{2} \left[\frac{a_o + v_o t'}{c} \right]^3 \right\} \times [\delta(t') - \delta(t'-T)] \right\}. \quad (29)$$

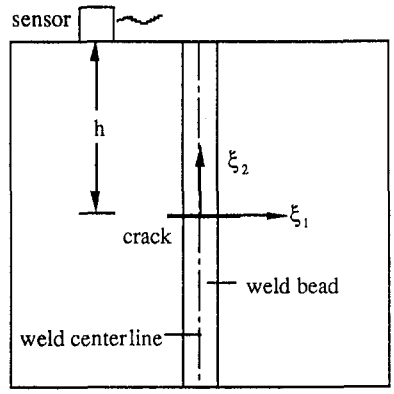

Fig. 5 Configuration of the weldment and vertical surface motion at the epicenter of the weldment

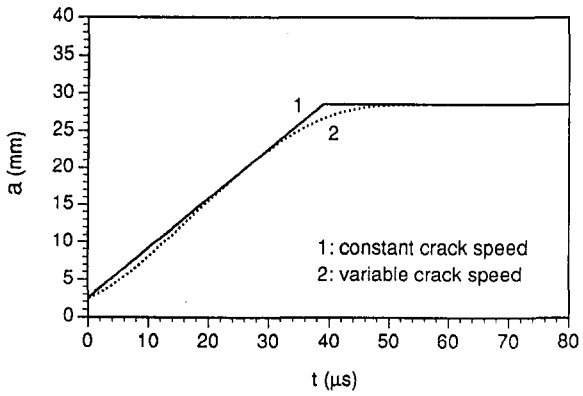

Fig. 6 Crack propagation models: (1) constant crack speed and (2) variable crack speed

For practical AE signal processing, the frequency response of the surface motion is of more interest. The magnitude spectrum for surface displacement is the magnitude of the Fourier transform of Eq. (28), i.e.,

$$\left| \frac{u_v(\omega)}{D} \right| = \frac{1}{D} \left| \int_{-\infty}^{\infty} u_v(t) e^{-i\omega t} dt \right| = \frac{v_o}{C_d[2-(a_o/c)^2]\sqrt{a_o/c}} \{A_1^2 + A_2^2 + A_3^2 + A_4^2 + Q\cos(\omega T + \Psi)\}^{1/2}, \quad (30)$$

where ω is the circular frequency, and

$$A_1 = \frac{v_o}{c\omega^2} - \frac{3v_o(a_o + v_oT)^2}{2c^3\omega^2} + \frac{3v_o^3}{c^3\omega^4},$$

$$A_2 = \frac{a_o + v_oT}{c\omega} - \frac{(a_o + v_oT)^3}{2c^3\omega} + \frac{3v_o^2(a_o + v_oT)}{c^3\omega^3},$$

$$A_3 = -\frac{v_o}{c\omega^2} + \frac{3a_o^2 v_o}{2c^3\omega^2} - \frac{3v_o^3}{c^3\omega^4},$$

$$A_4 = -\frac{a_o}{c\omega} + \frac{a_o^3}{2c^3\omega} - \frac{3a_o v_o^2}{c^3\omega^3}, \quad (31)$$

$Q = 2\sqrt{(A_1A_3 + A_2A_4)^2 + (A_1A_4 - A_2A_3)^2}$, and $\Psi = \cos^{-1}(2(A_1A_3 + A_2A_4)/Q)$.

Equations (30) and (31) show that the magnitude spectrum of surface motion depends on the initial crack length, crack speed, duration of crack propagation, and width of tension zone. It is evident that the shape of the magnitude spectrum is independent of the depth h.

Results for the special case of a weldment in 4340 steel with $c = 22.5$ mm, $a_o = 2.5$ mm, $v_o = 668.5$ m/s and $T = 39$ μs are studied. These parameters for the constant speed model (given by curve 1 in Fig. 6) were chosen to give as close a fit as possible to the variable speed predictions (given by curve 2 in Fig. 6) of Fang et al. (1993b). Figures 7(a) and 7(b) show the resulting vertical surface displacement and velocity, respectively.

The corresponding magnitude spectrum of surface displacement is given as curve 1 in Fig. 8(a), normalized with respect to the mean in the frequency range 0–1 MHz. An expanded view of the spectrum in the range 0–120 kHz is given in Fig.

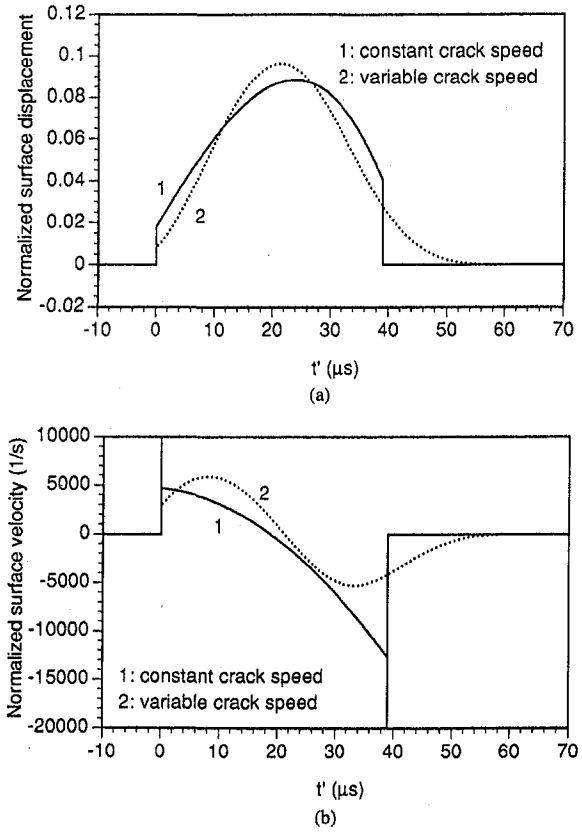

Fig. 7 Waveforms of far-field vertical surface motion at the epicenter of the weldment due to crack propagation: (*a*) displacement; (*b*) velocity a_o = 2.5 mm

8(*b*). The fluctuations observed in these curves are associated with the cosine term in Eq. (30) and their period is associated with the duration T of crack propagation.

6.2 Variable Crack Speed In practice, the crack speed will not be constant, but will be affected by the dynamic fracture process. Fang et al. (1993b) considered the problem of crack propagation in a nonuniform residual stress field, using an elastodynamic analysis of the instantaneous dynamic stress intensity factor and previously published experimental data for the relationship between dynamic fracture toughness and crack propagation speed. Their results lead to a differential equation that must be solved numerically and their results for variation of crack half-length with time are presented as curve 2 in Fig. 6. Using these results and Eq. (25), we obtain the surface motion due to variable speed crack propagation, which is shown as curves 2 in Figs. 7(*a, b*). The corresponding frequency response is shown in Figs. 8(*a, b*).

Figure 7 compares the surface motion at the epicenter in the time domain predicted by the constant crack speed and variable crack speed models. The duration of the wave for each curve corresponds to the crack propagation time. The difference in predicted surface displacement for these two models is minor except at crack arrest. As can be seen in Fig. 6, the crack arrest occurs abruptly in curve 1, but more smoothly in curve 2. This has a significant effect on the surface motion, particularly for surface velocity, where a spike is introduced at the end of curve 1 in Fig. 7(*b*) due to the sudden arrest of the crack. The difference is further manifested in the corresponding magnitude spectra of surface displacement, Fig. 8, which show that the variable crack speed spectrum has less high frequency components because the crack is arrested more smoothly as illustrated in Figs. 6 and 7.

6.3 Effect of Crack Length and Crack Bluntness. Fang et al. (1993b) showed that the propagation history is affected by the length of the initial crack and its bluntness. In particular, short and blunt cracks require a larger value of peak residual stress, σ_0, for the initiation of fracture, but the greater energy released during fracture then permits them to propagate more rapidly and results in longer crack extensions. We applied the propagation history (Fang et al. 1993b) to Eq. (24) to obtain AE surface response.

Figure 9 Shows the crack propagation histories for different initial crack lengths given by Fang et al. (1993b). The final crack half lengths are 32.3, 28.6, 24.8, 20.7, 20.5, and 23.1 mm for a_0 = 1, 2.5, 5, 10, 15, and 20, respectively. The effect of initial crack length on surface motion at the epicenter is illustrated in Figs. 10–12, which present displacement, velocity and magnitude spectra for displacement, respectively. The duration of the initial disturbance is equal to that of the crack propagation process.

The surface velocity (Fig. 11) exhibits a spike on the arrival of the P wave, followed by a period of oscillation equal to that of the crack propagation process. Both Figs. 10 and 11 show that the oscillatory behavior is most pronounced for short cracks, that for longer initial cracks (curves 4, 5, 6) being smaller. The frequency spectra (Fig. 12) show that a short initial crack has less high frequency components, while the difference at low frequencies has less engineering bearing since most standard AE systems starts at about 50 kHz.

Corresponding results for the effect of crack bluntness are presented in Figs. 14–16 based on the crack propagation histories in Fig. 13 given by Fang et al. (1993b). Here, all the results pertain to a crack of initial half length a_o = 2.5 mm. The final crack half lengths are 28.6, 30.4, 31.5, and 34.3 mm for n_b = 1, 1.5, 2, and 5, respectively. The results show that increasing

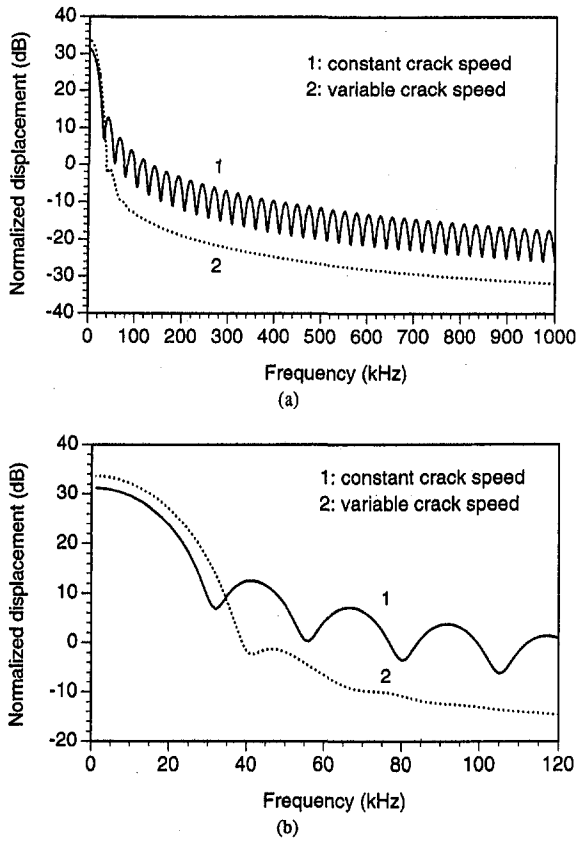

Fig. 8 Magnitude spectra of surface displacements at the epicenter due to crack propagation in the weldment: (*a*) overview; (*b*) details below 120 kHz, a_o = 2.5 mm

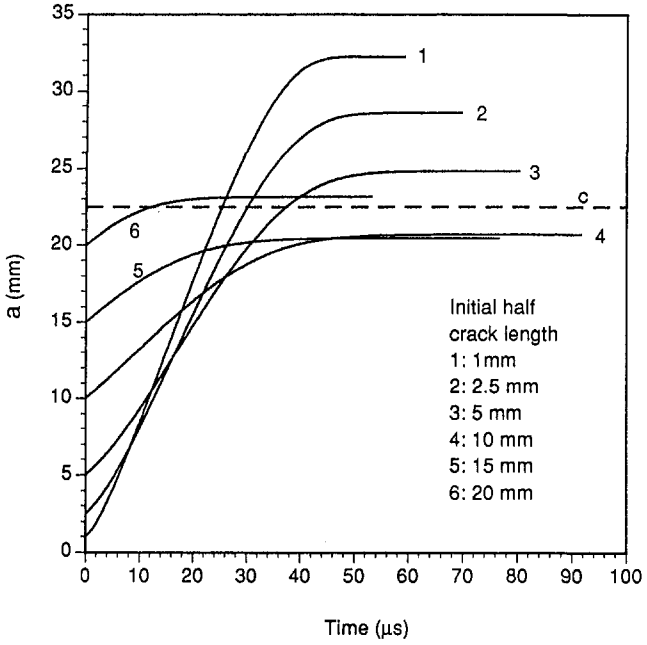

Fig. 9 Instantaneous crack length as a function of time for sharp cracks with different initial crack lengths subjected to a nonuniformly distributed residual stress in a 4340 steel plate (dashed line shows: $c = 22.5$ mm)

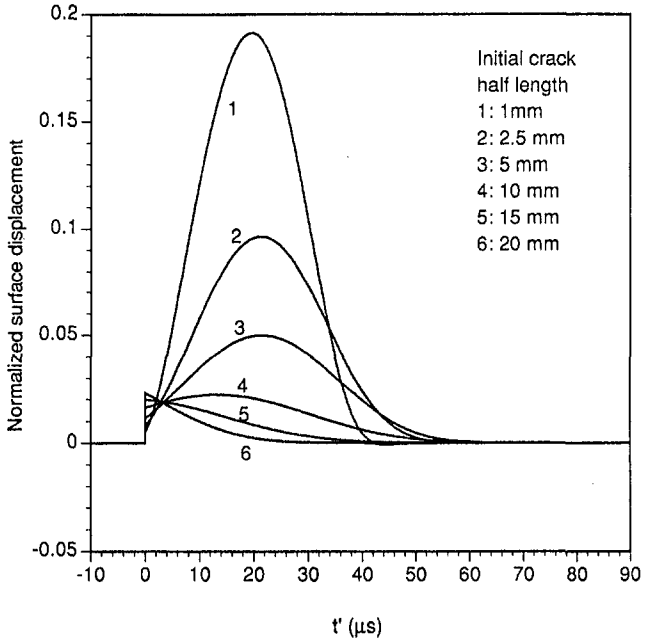

Fig. 10 Waveforms of normal surface displacements at the epicenter of the weldment due to the propagation of cracks with different initial crack lengths

bluntness acts in much the same way as reducing initial crack length. In particular, the magnitude of the surface motion is substantially increased and the shape of the disturbance becomes more oscillatory. This is particularly noticeable in Fig. 16, which shows that blunt cracks have more high frequency contents than a sharp crack.

7 Conclusions

The method described here permits the far-field AE sensor response to be determined as a function of the crack propagation rate, for cracking in a weldment subjected to non-uniform residual stresses. In particular, Eq. (25) gives the vertical surface displacement at the epicenter and Eq. (23) gives the corresponding expression for a more general point on the surface within a region defined by the inequalities (13) and (24).

Since the analysis is restricted to the direct (unreflected) initial P wave response, it is valid only until the first reflected P wave or the direct S wave reaches the sensor site. The AE signals recorded in practical tests are also influenced by the frequency response of the instrumentation, which must also therefore be taken into account in interpreting the results.

Theoretical predictions based on an earlier study (Fang et al., 1993b) of crack propagation due to residual stress in a

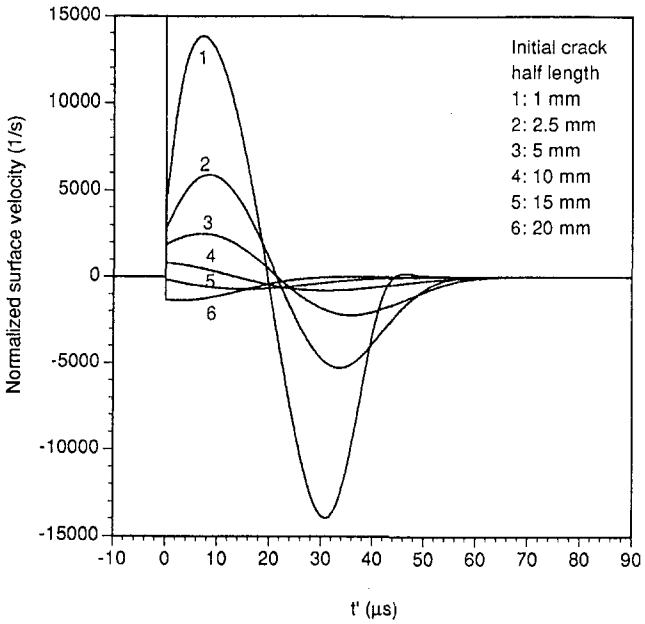

Fig. 11 Waveforms of normal surface velocities at the epicenter of the weldment due to the propagation of cracks with different initial crack lengths

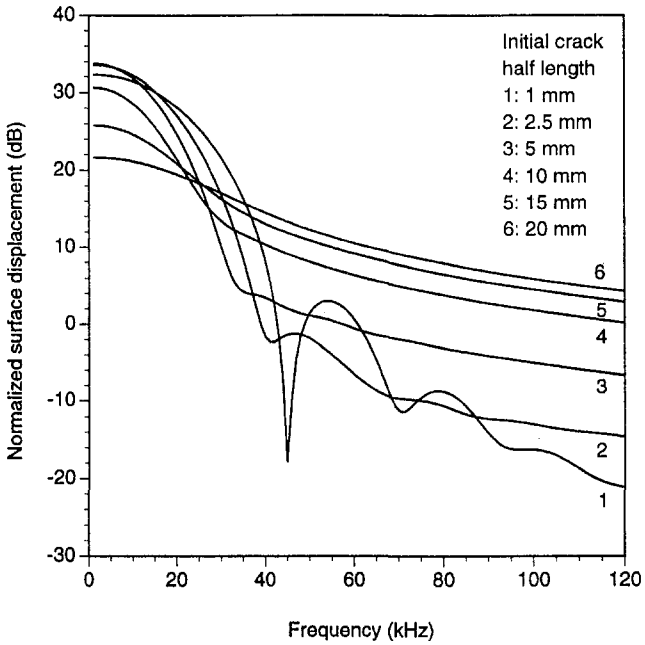

Fig. 12 Magnitude spectra of normal surface displacements at the epicenter of the weldment due to the propagation of cracks with different initial crack lengths

weldment show that short and/or blunt initial cracks produce large amplitude oscillatory surface motions, and their spectra contain more high frequency components. Longer sharp initial cracks produce a smaller amplitude surface velocity with an initial spike followed by oscillatory decay. However, long and/or blunt initial cracks contain more high frequency components in the spectra due to the more pronounced jump in the surface displacement corresponding to crack initiation.

A closed-form approximation to these results can be made by assuming that the crack propagates at uniform speed. If the average speed of the more exact analysis is used for the propagation speed, reasonable agreement is obtained, except that the approximation predicts a spike in the surface velocity at the point of crack arrest, which is not present in the more exact analysis. The spectra for the uniform speed model has more high frequency components since the crack is arrested more abruptly than the variable crack speed model.

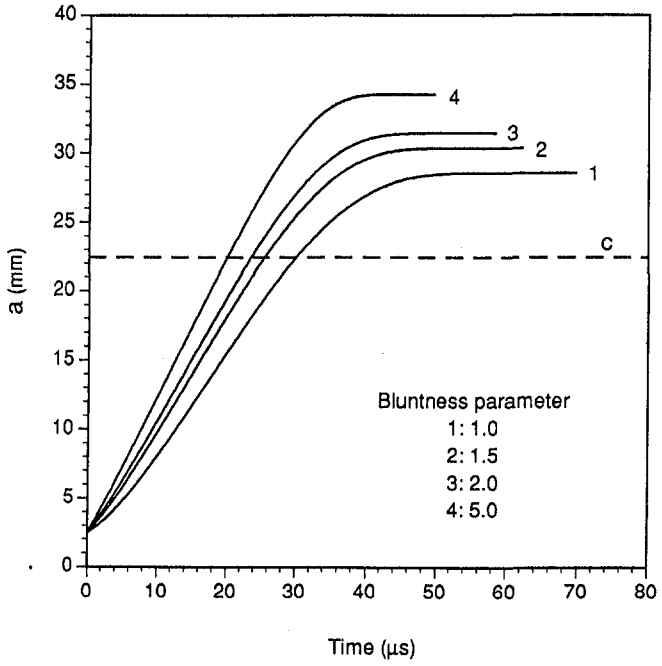

Fig. 13 Instantaneous crack length as a function of time for cracks, with the same initial crack length but different bluntness parameters, subjected to a nonuniformly distributed residual stress in a 4340 steel plate (dashed line shows c = 22.5 mm)

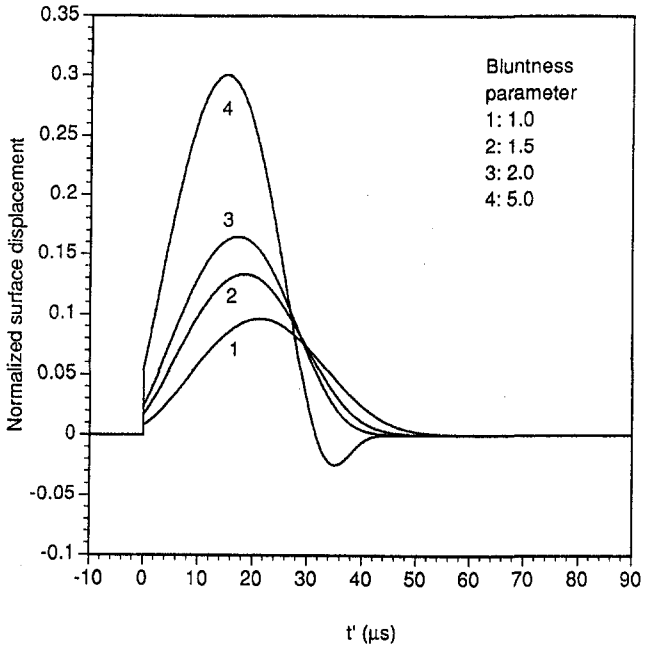

Fig. 14 Waveforms of normal surface displacements at the epicenter of the weldment due to the propagation of cracks with different bluntness parameters

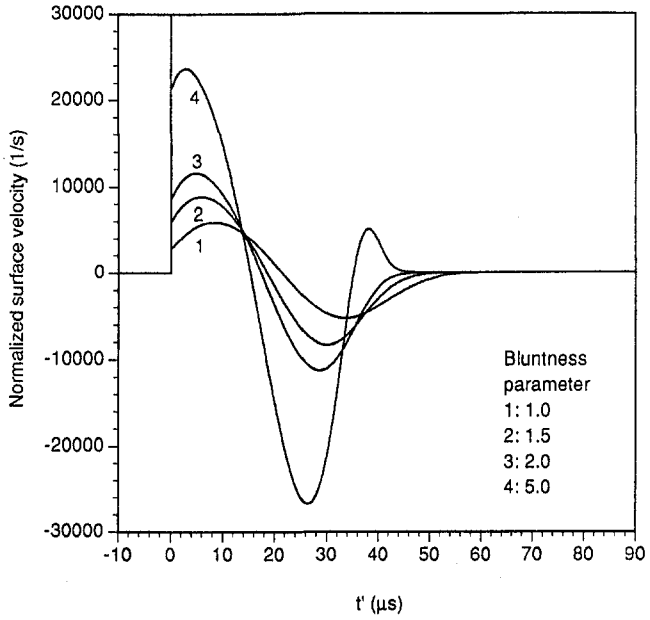

Fig. 15 Waveforms of normal surface velocities at the epicenter of the weldment due to the propagation of cracks with different bluntness parameters

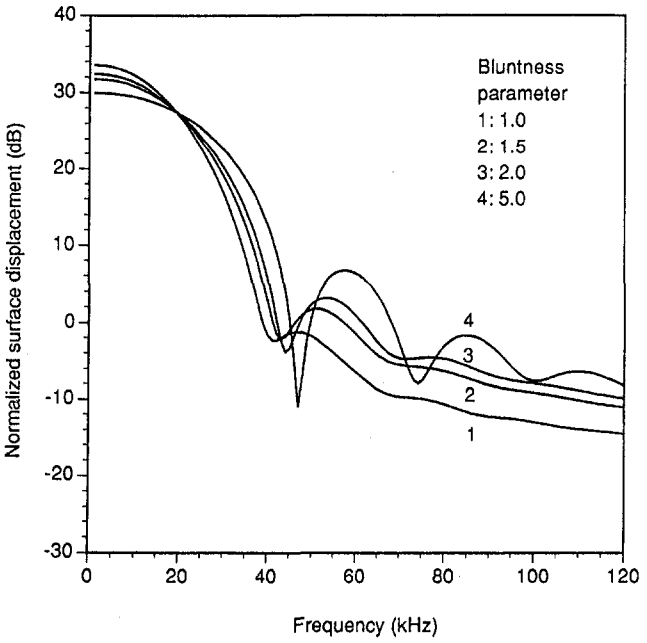

Fig. 16 Magnitude spectra of normal surface displacements at the epicenter of the weldment due to the propagation of cracks with different bluntness parameters

References

Aki, K., and Richards, P. G., 1980, *Quantitative Seismology Theory and Methods,* W. H. Freeman and Company, San Francisco.

Barber, J. R., 1992, *Elasticity,* Kluwer, Dordrecht.

Broek, D., 1986, *Elementary Engineering Fracture Mechanics,* 4th ed., Kluwer, Dordrecht.

Chen, C., and Sachse, W., 1988, "Quantitative Acoustic Emission Source Characterization of Fatigue Cracks in a Thin-Plate of 7075-T6 Aluminum," *J. Appl. Phys.,* Vol. 64, No. 11, December, pp. 6264–6273.

Enoki, M., Kishi, T., Kihara, J., and Kohara, S., 1986, "Determination of Microcracking Moment Tensor of Quasi-cleavage Facet by AE Source Characterization," *Progress in Acoustic Emission III,* The Japanese Society of NDI, pp. 763–770.

Enoki, M., and Kishi, T., 1988, "Theory and Analysis of Deformation Moment Tensor Due to Microcracking," *International Journal of Fracture,* Vol. 38, pp. 295–310.

Fang, C.-K., Kannatey-Asibu Jr., E., and Barber, J. R., 1993a, "Acoustic Emission as a Function of Crack Opening Displacement in a Half-Space," submitted to ASME *Journal of Engineering Materials and Technology.*

Fang, C.-K., Kannatey-Asibu Jr., E., and Barber, J. R., 1993b, "Crack-tip Equation of Motion due to Non-uniform Residual Stresses in a Weldment," submitted to *Welding Journal.*

Hirose, S., and Achenbach, J. D., 1991, "Acoustic Emission and Near-Tip Elastodynamic Fields of a Growing Penny-Shaped Crack," *Engineering Fracture Mechanics,* Vol. 39, No. 1, pp. 21–36.

Kishi, T., and Ohira, T., 1983, "Dynamic Crack Growth During Pop-in Fracture in 7075 Aluminum Alloy," *Transactions of the Japan Institute of Metals,* Vol. 24, No. 4, pp. 255–263.

Liptai, R. G., and Tatro, C. A., 1976, "Acoustic-Emission Inspection," *Metals Handbook,* 8th edn., Vol. 11, p. 234–243.

Masubuchi, K., 1960, "Analytical Investigation of Residual Stresses, and Distortions Due to Welding," *Welding Journal,* December, pp. 525s–537s.

Masubuchi, K., and Martin, D. C., 1966, "Investigation of Residual Stresses by Use of Hydrogen Cracking - Part II," *Welding Journal,* Vol. 45, No. 9, Research Supplement, pp. 401s–418s.

Masubuchi, K., 1980, *Analysis of Welded Structures,* Pergamon Press, New York.

Ohtsu, M., and Ono, K., 1984, "A Generalized Theory of Acoustic Emission and Green's Functions in a Half Space," *Journal of Acoustic Emission,* Vol. 3, No. 1, pp. 27–40.

Ohtsu, M., Yuyama, S., and Imanaka, T., 1987, "Theoretical Treatment of Acoustic Emission Sources in Microfracturing due to Disbonding," *Journal of the Acoustical Society of America,* Vol. 82, No. 2, pp. 506–512.

Rice, J. R., 1980, "Elastic Wave Emission from Damage Processes," *Journal of Nondestructive Evaluation,* Vol. 1, No. 4, pp. 215–224.

Tatsukawa, I., and Oda, I., 1972, "Distortions and Residual Stresses in Arc Welding," *Transactions of the Japan Welding Society,* Vol. 3, No. 2, pp. 37–46.

Wadley, H. N. G., Scruby, C. B., and Shrimpton, G., 1981, "Quantitative Acoustic Emission Source Characterisation During Low Temperature Cleavage and Intergranular Fracture," *Acta Metallurgica,* Vol. 29, pp. 399–414.

Wadley, H. N. G., and Scruby, C. B., 1983, "Elastic Wave Radiation from Cleavage Crack Extension," *International Journal of Fracture,* pp. 111–128.

Wakayama, S., and Kishi, T., 1985, "Quantitative Evaluation of Microcrackings During Fracture Toughness Testing of Al_2O_3 by AE Source Characterization," Special Supplement to *Journal of Acoustic Emission,* Vol. 4, pp. S278–281.